Relationship between the structural and magnetic properties of Co-doped SnO_2 nanoparticles

J. Hays and A. Punnoose*
Department of Physics, Boise State University, Boise, Idaho 83725, USA

R. Baldner
Analytical Chemistry Lab, Micron Technology, Boise, Idaho 83707, USA

M. H. Engelhard
Environmental Molecular Sciences Laboratory, Pacific Northwest National Laboratory, Richland, Washington 99352, USA

J. Peloquin
Department of Chemistry, Boise State University, Boise, Idaho 83725, USA

K. M. Reddy
Department of Physics, Boise State University, Boise, Idaho 83725, USA
(Received 2 September 2004; revised manuscript received 27 May 2005; published 5 August 2005)

In this paper, we present the results of a detailed investigation of the structural, optical, and magnetic properties of chemically synthesized pure and Co-doped SnO_2 powders using x-ray diffraction (XRD), diffuse reflectance spectroscopy, Raman spectroscopy, x-ray photoelectron spectroscopy, and magnetometry. In $Sn_{1-x}Co_xO_2$ samples prepared at 600 °C with low doping concentrations of Co ($\leqslant 1\%$), the SnO_2 lattice contracts, band gap energy decreases, and a ferromagnetic behavior is developed. Increasing the Co doping concentration to $>1\%$ leads to a rapid expansion of the lattice and significant structural disorder evidenced by changes in the XRD and Raman spectra presumably due to additional interstitial incorporation of Co. This higher Co doping completely destroys the ferromagnetism. The striking similarity between the changes in the lattice parameters and the magnetic properties of $Sn_{1-x}Co_xO_2$ indicates a structure-magnetic property relationship.

DOI: 10.1103/PhysRevB.72.075203 PACS number(s): 75.50.Pp, 75.50.Tt, 75.50.Dd, 75.30.Cr

I. INTRODUCTION

Tin dioxide is a very interesting oxide semiconductor with a wide band gap of ~3.6 eV. Its high optical transparency, electrical conductivity, and chemical sensitivity make it a very attractive material for solar cells, heat mirrors, catalysis, and gas-sensing applications. Tailoring the physical properties and adding new functionalities to the existing semiconductors by engineering the structure, composition, and particle/grain size are among the new approaches in advancing the current applications of semiconductor materials. Preparation of these materials in the nanoscale size range is more interesting due to the increased surface-to-volume ratio which might affect the structural and most other physical properties. Transition-metal (TM) doping has been proposed to introduce magnetic functionality in conventional semiconductors.[1,2] Recent reports on the observation of room-temperature ferromagnetism (RTFM) in thin films of TM-doped oxide semiconductors such as TiO_2,[3–6] ZnO,[5–8] and SnO_2 (Refs. 9–11) generated tremendous interest in investigating these materials. In the nanoscale form, these materials are reported to demonstrate more interesting magnetic properties.[6] For example, Co-doped TiO_2 nanocrystals were paramagnetic when prepared as isolated particles, but showed weak ferromagnetism when aggregated, and strong ferromagnetism in spin coated thin film form.[6]

In a very recent work,[9] we have shown that chemically synthesized $Sn_{1-x}Co_xO_2$ powders exhibit RTFM for $x \leqslant 0.01$ when prepared in the 350 to 600 °C range. However, for $x>0.01$, this ferromagnetism was completely destroyed and the samples demonstrated a paramagnetic behavior. Here we report detailed investigations of the structural, optical, and magnetic properties of pure and Co-doped nanoparticles of SnO_2 with a specific interest to understand why >1% Co doping destroyed the observed ferromagnetism. The structural and optical investigations reported in this work are carried out on 600 °C prepared $Sn_{1-x}Co_xO_2$ samples to avoid any pure or doped SnO inclusions that might form at lower preparation temperatures.

II. EXPERIMENTAL

Pure and Co-doped SnO_2 powders were synthesized by reacting appropriate amounts of $SnCl_2$ and $CoCl_2 \cdot 6H_2O$ at 80 °C followed by annealing the dried precipitate in air at different temperatures for 3 h. Detailed characterization of the samples using transmission electron microscopy (TEM), electron diffraction, and x-ray diffraction (XRD) showed the formation of $Sn_{1-x}Co_xO_2$ when prepared by annealing the precipitate in the 350 to 830 °C range.[9] The nominal Co doping concentrations were confirmed by particle induced x-ray emission (PIXE) measurements carried out in the accelerator facility at Pacific Northwest National Laboratory. Details of these synthesis and characterization studies of the samples have been reported in Ref. 9. XRD spectra were

recorded at room temperature on a Phillips X'Pert x-ray diffractometer with a Cu K_α source ($\lambda = 1.5418$ Å) in Bragg-Brentano geometry. The loose powder samples were leveled in the sample holder to ensure a smooth surface and mounted on a fixed horizontal sample plane. Data analyses were carried out using profile fits of selected individual XRD peaks. Room-temperature optical spectra in the ultraviolet and visible light wavelength ranges were collected using a CARY 5000 spectrophotometer fitted with an integrating sphere diffuse reflectance accessory. The spectrophotometer measures reflectance relative to a background scatterer, which was powdered $BaSO_4$. Raman spectra were collected using a Renishaw S2000 Raman microscope. Samples were all probed using identical instrument conditions: 783 nm diode laser, 1200 line/mm grating, over a Stokes Raman shift range of 50–1000 cm^{-1}. A line focus accessory was also employed, which permitted the collection of photon scatter data from an area ~ 2 μm by 60 μm, rather than a discreet 1–2 μm diameter spot. Incident laser power was not measured, however, power at laser head was ~ 28 mW, which would be expected to produce ~ 2–4 mW at the sample. Sample preparation consisted of loosely packing the powder into a stainless steel die accessory, which was then mounted on the microscope stage for probing. X-ray photoelectron spectroscopy (XPS) measurements were performed using a Physical Electronics Quantum 2000 Scanning ESCA Microprobe. This system uses a focused monochromatic Al K_α x-ray (1486.7 eV) source and a spherical section analyzer. The instrument has a 16 element multichannel detector. The x-ray beam used was a 105 W, 100 μm diameter beam that was rastered over a 1.4 by 0.2 mm rectangle on the sample. The x-ray beam was incident normal to the sample and the photoelectron detector was at 45° off normal. The data were collected using a pass energy of 46.95 eV. For the Ag $3d_{5/2}$ line, these conditions produce full widths at half maximum (FWHM) of better than 0.98 eV. Although the binding energy (BE) scale was calibrated using the Cu $2p_{3/2}$ feature at 932.62 ± 0.05 eV and Au $4f$ feature at 83.96 ± 0.05 eV for known standards, the Co-doped SnO_2 surface experienced variable degrees of charging. Low-energy electrons at ~ 1 eV, 21 μA and low-energy Ar^+ ions were used to minimize this charging. The BE positions were referenced using the 486.7 eV position for the Sn $3d_{5/2}$ feature. Magnetic measurements were carried out as a function of temperature (4 to 300 K) and magnetic field (0 to ± 65 kOe) using a commercial magnetometer (Quantum Design, PPMS) equipped with a superconducting magnet. Measurements were carried out on tightly packed powder samples placed in a clear plastic drinking straw. The data reported here were corrected for the background signal from the sample holder independent of magnetic field and temperature. In all these experiments, the samples were run without mixing with any contaminants.

III. EXPERIMENTAL RESULTS AND DISCUSSION

A. X-ray diffraction studies

XRD patterns of the $Sn_{1-x}Co_xO_2$ samples[9] showed the formation of tetragonal cassiterite SnO_2 with a very small fraction of metastable orthorhombic phase. For $x \geqslant 0.08$, weak peaks of Co_3O_4 started appearing and gradually strengthened with increasing Co doping, suggesting a saturation limit of Co in SnO_2. It is noted that with increasing Co concentration, the intensity of the cassiterite SnO_2 phase decreased while the relative concentration of the orthorhombic phase gradually increased. Changes in the XRD peak intensity of the cassiterite phase (I_{c110}) and the orthorhombic phase fraction (x_o) of SnO_2 are shown in Fig. 1(a). The orthorhombic fraction x_o was calculated using the method of standard additions[12] $x_o = K/[K + (I_{c110}/I_{o111})]$, using $K = 2.69$.[13] Formation of the high-temperature orthorhombic

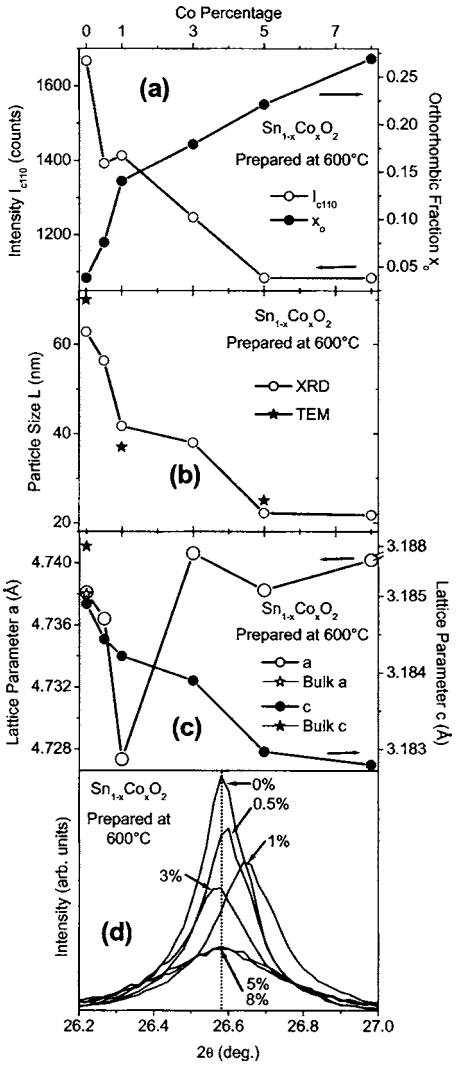

FIG. 1. (a) Intensity of the tetragonal cassiterite peak (110) and the orthorhombic fraction x_o of $Sn_{1-x}Co_xO_2$ prepared at 600 °C as a function of Co percentage. (b) The particle size of $Sn_{1-x}Co_xO_2$ as a function of x calculated from the XRD tetragonal cassiterite peak (110). The particle sizes determined from TEM are marked with stars. (c) Changes in the lattice parameters a and c of cassiterite SnO_2 as a function of Co percentage. Stars indicate the bulk values of the SnO_2 lattice parameters from XRD reference files. (d) Changes in the (110) cassiterite peak position with Co concentration. The lattice parameters were calculated using (110) and (202) peaks of the tetragonal cassiterite phase.

SnO_2 phase at ambient conditions has been observed in thin films[14,15] and nanoscale powders.[16] Nucleation of the metastable orthorhombic phase has been attributed to thin film strains[14,15] and size-dependent internal pressures due to surface stresses in nanoparticles.[16] Therefore, the increasing orthorhombic fraction of SnO_2 with Co concentration indicates that Co doping causes structural disorder and strain, and possible changes in the particle size. The growth of the orthorhombic fraction is fast up to 1% Co, above which a slower growth is observed [Fig. 1(a)]. This suggests that the intrinsic doping mechanisms active in the Co concentration regimes above and below 1% may be different.

The average particle size L of the tetragonal SnO_2 phase was calculated using the width of the (110) peak and the Scherrer relation $L=0.9\lambda/B\cos\theta$ [where θ is the peak position, λ is the x-ray wavelength, and $B=(B_m^2-B_s^2)^{1/2}$ was estimated using the measured peak width B_m and the instrumental width B_s]. These estimates showed that the crystallite size decreased with Co doping, as shown in Fig. 1(b), in excellent agreement with our recent TEM studies.[9] TEM images of pure and 1% Co-doped SnO_2 samples showed nearly spherical nanoparticles. 1% Co doping reduced the average size of the SnO_2 particles to ~37 nm which is about half the average size of the pure SnO_2 particles (~70 nm) prepared under similar conditions. On increasing the Co concentration to 5%, the average particle size was further reduced to 25 nm. This indicates that Co doping inhibits the growth of SnO_2 nanoparticles.

XRD peak positions showed significant changes with Co doping as shown in Figs. 1(c) and 1(d). The tetragonal cassiterite SnO_2 peaks initially shifted to the higher 2θ angles as x increased to 0.01 [Fig. 1(d)]. But for $x=0.03$, there is a dramatic shift to the lower angles followed by moderate changes in the peak positions at higher x. These changes revealed interesting variations in the lattice parameters a and c with Co concentration as shown in Fig. 1(c). The SnO_2 lattice parameter a initially decreased due to Co doping for $x\leqslant 0.01$. Such a rapid contraction of the lattice can be understood qualitatively considering the sizes of the ions and their local coordinations. Substitution of 0.69 Å sized Sn^{4+} ions with 0.58 Å sized Co^{2+} ions[17] is expected to reduce the interatomic spacing significantly, justifying the initial contraction of the lattice for $x\leqslant 0.01$. The observed rapid expansion of the lattice for $x=0.03$ indicates a significantly different doping mechanism. At higher doping concentrations, the incorporation of dopant ions in interstitial sites has been reported in some host systems causing somewhat similar structural changes in the lattice parameters.[17] Interstitial incorporation of Co^{2+} ions might cause significant changes and disorder in the SnO_2 structure as well as many dramatic changes in the properties of the material, discussed in the following sections. The large difference in the charges and coordination numbers of Sn^{4+} and Co^{2+} ions will also contribute to the structural disorder in SnO_2 due to the removal of some oxygen ions that were attached to the octahedrally coordinated Sn^{4+}. For $x\geqslant 0.03$, the observed expansion along the a direction and continued contraction along the c direction [Fig. 1(c)] will contribute to changes in the shape of the SnO_2 lattice and the nanoparticles. This was indeed observed in the TEM measurements reported before.[9] On increasing the Co concentration to 5%, the spherical SnO_2 particles (observed in the undoped as well as 1% Co doped samples) appeared as nanorods with an aspect ratio as high as 3.

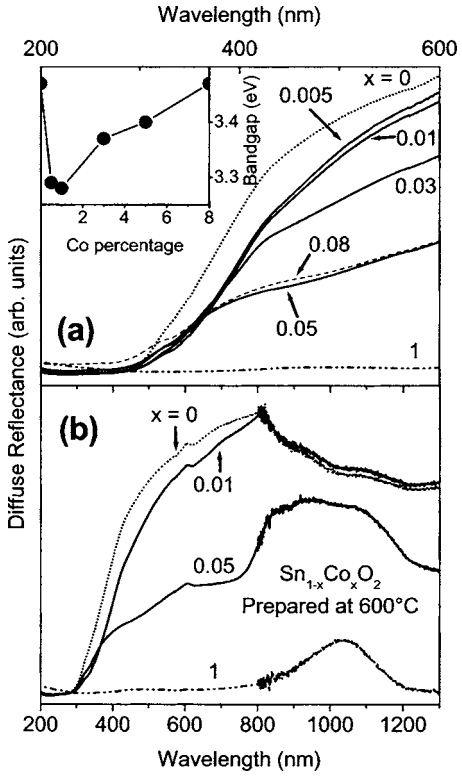

FIG. 2. Diffuse reflectance spectra of $Sn_{1-x}Co_xO_2$ samples prepared at 600 °C. (a) The changes in the absorption edge with Co concentration; inset in panel (a) shows the changes in the band gap energy estimated from the reflectance data as a function of Co concentration and (b) shows the complete spectra indicating the extent of Co_3O_4 formation.

B. Optical measurements

Preliminary optical characterization of the pure and Co-doped SnO_2 powders were carried out by measuring the diffuse reflectance at room temperature. Figure 2(a) shows a shift of the absorption edge to longer wavelengths/lower energies and a decrease in the band gap of SnO_2 for $x\leqslant 0.01$. Increasing the Co doping above this level reversed the trend in that the band gap increased gradually and a reduction in the reflectance was observed with Co percentage. The diffuse reflectance, R, of the sample is related to the Kubelka-Munk function $F(R)$ by the relation $F(R)=(1-R)^2/2R$, where R is the percentage reflectance.[18] The spectra used for the bandgap calculations are plotted in terms of $F(R)$. The bandgap energy of the $Sn_{1-x}Co_xO_2$ powders were calculated from their diffuse-reflectance spectra by plotting the square of the Kubelka-Munk function $F(R)^2$ vs energy in electron volts. The linear part of the curve was extrapolated to $F(R)^2=0$ to get the direct bandgap energy. Such shifts of the absorption edge and band gap energy due to TM doping have been recently reported in Co- (Ref. 10) and Mn-doped (Ref. 19) SnO_2 thin films, as well as other TM-doped semiconductor

systems.[20,21] For example, Schwartz *et al.* observed an increase in the band gap energy and decrease in the band gap intensity of Co-doped ZnO nanoparticles with increasing Co concentration.[21]

Diffuse reflectance measurements carried out on pure nanoscale Co_3O_4 reference sample prepared using an identical procedure (with $x=1$), showed prominent signatures at lower energies as shown in Fig. 2(b). Comparison of the optical spectra of $Sn_{1-x}Co_xO_2$ samples with this suggests that samples with $x \leqslant 0.01$ do not have any Co_3O_4 phase. However, evidence of its presence was observed in all samples with $x \geqslant 0.03$. This indicates that in samples with $x=0.03$ and 0.05, at least a fraction of the Co atoms precipitate as Co_3O_4 although XRD shows its formation only for $x \geqslant 0.08$. Since the detection limit of the x-ray diffractometer employed was ~1.5% [determined from XRD measurements of the physical mixtures of SnO_2 ($x=0$) and Co_3O_4 ($x=1$) nanoparticles prepared under identical synthesis conditions], the fraction of Co forming Co_3O_4 in 3 and 5 % Co-doped SnO_2 should only be below this level. This explains why the lattice parameters, band gap, particle size, shape, and orthorhombic/tetragonal fractions continue to change for $x>0.01$ although the changes are relatively smaller in this range as illustrated in Figs. 1 and 2.

C. Raman spectroscopy measurements

Figure 3(a) shows the Raman spectra of $Sn_{1-x}Co_xO_2$ samples as a function of Co concentration. The pure SnO_2 spectrum [Figs. 3(a) and 3(b)] shows the classic cassiterite SnO_2 vibrations at 476, 630, and 776 cm^{-1}.[22] Addition of 0.5 or 1.0 mol. % Co results in the appearance of two new peaks at 300 and 692 cm^{-1}. However, no significant change in the SnO_2 peak positions or widths were observed for these doping concentrations. These new Raman peaks at 300 and 692 cm^{-1} may be due to the vibrational modes activated by local structural changes resulting from the substitution of Co^{2+} ions at the Sn^{4+} sites. Further addition of Co to 3 or 5 mol. %, results in the appearance of peaks at 196, 480, 520, 617, and 688 cm^{-1}. These five peaks observed in the samples with $x \geqslant 0.03$ match well with published Raman data of Co_3O_4.[23,24] The appearance of Co_3O_4 vibrational modes is in good agreement with the result from the optical data that predicts at least a fraction of the doped Co precipitates out as Co_3O_4 for $x \geqslant 0.03$.

For $Sn_{1-x}Co_xO_2$ samples with $x \geqslant 0.03$, there is an apparent disappearance of the SnO_2 peaks. This disappearance is most obvious for the 630 cm^{-1} SnO_2 peak as illustrated in Fig. 3(c) and would suggest a loss of the SnO_2 phase. However, the 776 cm^{-1} SnO_2 peak is still visible in the 3 and 5 % Co-doped samples. At best, its intensity has diminished by a factor of 2. The extensive peak broadening and the subsequent disappearance of the 630 cm^{-1} peak and the loss in intensity of the 776 cm^{-1} peak are indicative of significant structural modifications and disorder of the SnO_2 lattice for $x \geqslant 0.03$. Based on the drastic changes observed in the lattice parameter a, particle size, and particle shape, this disappearance of the Raman peak also may be due to the interstitial incorporation of Co^{2+} ions and the subsequent structural changes.

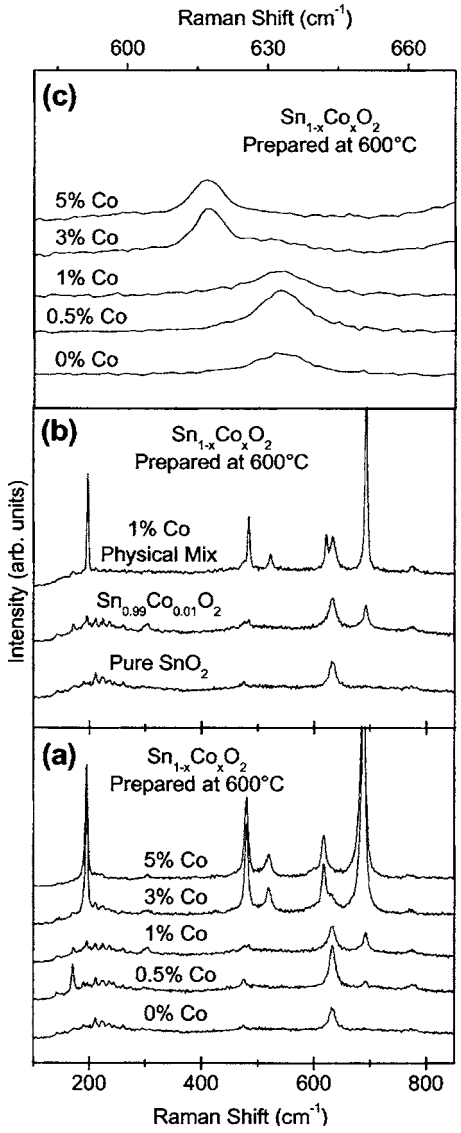

FIG. 3. (a) Raman spectra of $Sn_{1-x}Co_xO_2$ prepared at 600 °C as a function of x. (b) Raman spectra of pure SnO_2, 1% Co-doped SnO_2 and a physical mixture of pure SnO_2 and Co_3O_4. (c) The apparent disappearance of SnO_2 Raman peak at 630 cm^{-1} and the emergence of the 617 cm^{-1} peak of Co_3O_4 for $x>0.01$.

As discussed above, at 0.5 and 1 mol. % of Co, a small Raman peak is present at 692 cm^{-1}. However, when the Co mol. % is increased to 3, an intense Raman peak at 688 cm^{-1} appears. The width of the 688 cm^{-1} peak precludes determination if the 692 cm^{-1} is still present. Two obvious conclusions are possible: (i) the 692 cm^{-1} peak represents a very small amount of Co_3O_4 and (ii) the 692 cm^{-1} mode represents a vibrational mode of $Sn_{1-x}Co_xO_2$. Figure 3(b) compares the Raman spectra of undoped SnO_2 and 1% Co-doped SnO_2 (both prepared at 600 °C through identical procedures) and the Raman spectrum of a physical mixture of SnO_2 and Co_3O_4 with 1 mol. percent Co (both prepared separately at 600 °C). For the physical mixture, no annealing was performed following the mixing. The Raman spectrum of the physical mixture is clearly a superposition of a SnO_2 spectrum and a Co_3O_4 spectrum. It is also clear that the intensity

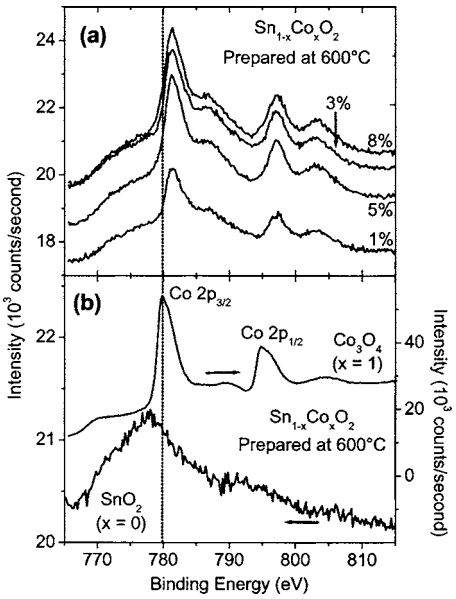

FIG. 4. (a) XPS spectra of $Sn_{1-x}Co_xO_2$ prepared at 600 °C as a function of Co percentage and (b) shows similar data of Co_3O_4 ($x=1$) and SnO_2 ($x=0$) reference samples prepared under identical synthesis conditions.

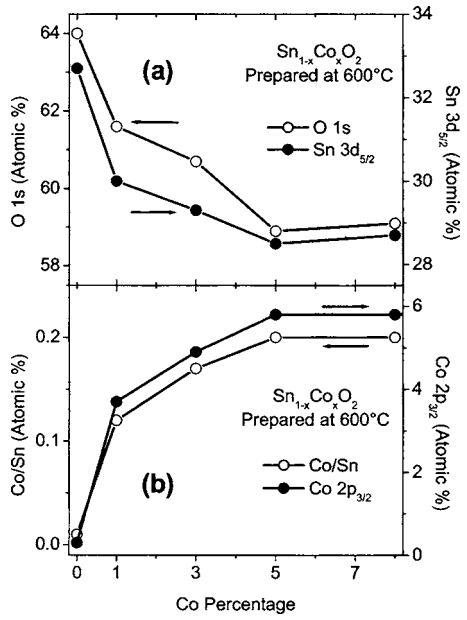

FIG. 5. (a) and (b) The variation of the atomic percentages of Co, Sn, and O and the Co/Sn ratio as a function of Co concentration calculated using the corresponding XPS peak intensities.

of the SnO_2 peaks in the undoped SnO_2, the 1% Co-doped SnO_2 and the physical mixture samples are essentially the same. This indicates that the same percentage of SnO_2 in the cassiterite form is present in all three samples. The intensity of the 692 cm^{-1} peak in the 1% doped sample is roughly 1/10 that of the 688 cm^{-1} peak in the physical mixture. This disparity in intensity suggests that even if we assign the 692 cm^{-1} peak to traces of Co_3O_4, then there is no more than 0.1% Co_3O_4 in the 1% Co-doped sample.

D. XPS measurements

The Co $2p_{3/2}$ and Co $2p_{1/2}$ XPS spectral region of the $Sn_{1-x}Co_xO_2$ samples are shown in Fig. 4. Comparing the binding energies of the Co primary and satellite XPS peaks with that observed for Co(0) in Co metal, Co^{2+} in CoO, and Co^{3+} in γ-Co_2O_3,[25,26] the electronic state of Co in $Sn_{1-x}Co_xO_2$ samples is found to be Co^{2+} and that it is not bonded to oxygen as CoO or Co_3O_4. It also rules out any metallic Co clusters in the samples, a result well expected for chemically synthesized samples prepared and processed in air. These results agree well with the 2+ oxidation state of Co with $S=3/2$ determined from magnetization measurements of paramagnetic samples of $Sn_{1-x}Co_xO_2$.[9] The $\geqslant 1$ eV shift of the Co $2p_{3/2}$ peak in the $Sn_{1-x}Co_xO_2$ samples compared to that observed from the Co_3O_4 reference sample suggests that Co is indeed incorporated in the SnO_2 lattice and not forming any significant amount of Co oxides. However, no significant change in the Co binding energy is observed with increasing Co doping concentration. Careful analysis of the peak positions of the Sn $3d_{5/2}$ (486.7 eV) and O 1s (530.65 eV) peaks also did not show any noticeable change in the binding energy with increasing Co concentration.

Atomic percentages of Sn, Co, and O calculated using the Sn $3d_{5/2}$ (486.7 eV), O 1s (530.65 eV), and Co $2p_{3/2}$ (781.4 eV) peaks are shown in Fig. 5. In these plots, three well defined regions are present. A rapid increase in the atomic percentage of Co and the Co/Sn ratio, and a decrease in the Sn atomic percentage for $x \leqslant 0.01$ indicate substitutional incorporation of Co at Sn sites. In the $0.01 \leqslant x \leqslant 0.05$ range, a relatively slower variation is observed suggesting more interstitial incorporation and/or Co_3O_4 precipitation in agreement with results form XRD, Raman, and optical studies, discussed above. In the case of substitutional Co incorporation, Co ions remove Sn ions from the SnO_2 structure. However, in the case of interstitial incorporation or Co_3O_4 precipitation, there is no Sn removal. For $x > 0.05$, changes in the Co/Sn atomic percentage ratio are minimal indicating lack of further Co incorporation into the SnO_2 lattice. Estimation of the oxygen content in the samples using the O 1s (530.65 eV) peak indicated almost stoichiometric Sn/O ratio for the undoped sample. Co doping decreases the oxygen content of the sample as shown in Fig. 5(a). Removal of oxygen atoms from the SnO_2 lattice is well expected if Co^{2+} replaces Sn^{4+} ions due to charge neutrality requirements. It has been argued[5] that substitutional Co^{2+} and oxygen vacancies in excess of those necessary for charge neutrality are essential to produce ferromagnetism in $Ti_{1-x}Co_xO_2$. A rapid loss in oxygen content, indicated by relatively larger changes in the oxygen atomic percentage, for samples with $x \leqslant 0.01$ [Fig. 5(a)], may be crucial for the ferromagnetism observed only in this narrow Co percentage range of $\leqslant 1\%$.

E. Magnetic measurements

Magnetic measurements carried out on pure SnO_2 nanoparticles showed the expected diamagnetism with a negative magnetic susceptibility. In Ref. 9, we have shown that the $Sn_{1-x}Co_xO_2$ samples with $x \leqslant 0.01$ were all ferromagnetic at

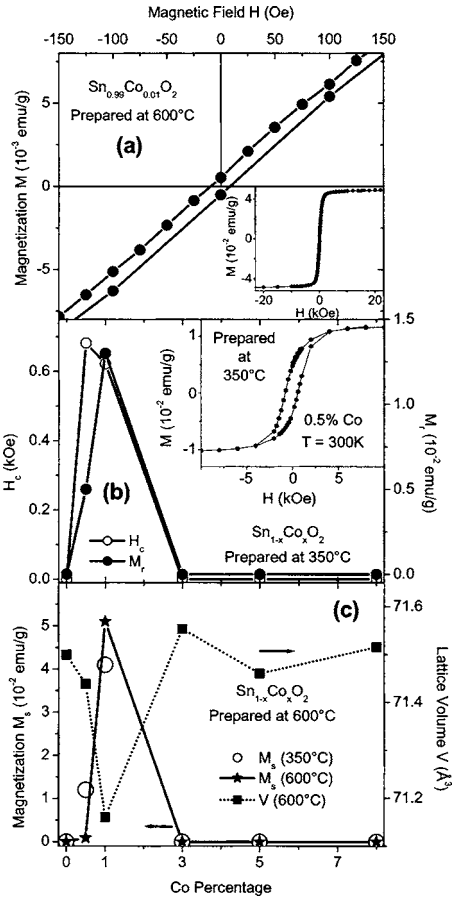

FIG. 6. (a) The low field region of the room-temperature hysteresis loop of 600 °C prepared $Sn_{0.99}Co_{0.01}O_2$ sample showing a coercivity of 9 Oe; the inset in (a) shows the complete hysteresis loop of 600 °C prepared $Sn_{0.99}Co_{0.01}O_2$ showing saturation of the sample magnetization expected for a ferromagnetic system, (b) variation of the room-temperature coercivity H_c and remanence M_r of $Sn_{1-x}Co_xO_2$ prepared at 350 °C as a function of x; inset in (b) shows the expanded view of the low-field region of the hysteresis loop of 350 °C prepared $Sn_{0.995}Co_{0.005}O_2$ sample, and (c) variation of the saturation magnetization M_s with x of $Sn_{1-x}Co_xO_2$ samples prepared at 350 (open circles) and 600 °C (solid stars), and the lattice volume V calculated using the a and c values of Fig. 1(c) (shown with solid squares) as a function of Co-doping concentration for the 600 °C prepared $Sn_{1-x}Co_xO_2$.

room temperature when prepared in the 350 to 600 °C temperature range. Figure 6(a) shows the room-temperature hysteresis loop measured from a $Sn_{0.99}Co_{0.01}O_2$ sample prepared at 600 °C illustrating a clear ferromagnetic behavior with a coercivity $H_c=9$ Oe. In Fig. 6(b), the variations of the room-temperature coercivity H_c and remanence M_r of 350 °C prepared $Sn_{1-x}Co_xO_2$ as a function of Co concentration are shown. The observed coercivities of ~630 Oe and remanences as high as 31% are among the highest reported for dilute magnetic semiconductors. The observed variation of the saturation magnetization M_s with Co concentration measured from the $Sn_{1-x}Co_xO_2$ samples prepared at 350 and 600 °C were comparable as illustrated in Fig. 6(c). However, the coercivities of the $Sn_{0.99}Co_{0.01}O_2$ samples decreased from 630 to 9 Oe as the preparation temperature increased from 350 to 600 °C [see Figs. 6(a) and 6(b)].[9] This most likely indicates a change in the magnetocrystalline anisotropy due to reasons that are unclear at present. More importantly, irrespective of the preparation temperature, all $Sn_{1-x}Co_xO_2$ samples prepared in the 350 to 600 °C showed complete destruction of the ferromagnetism above 1% Co doping and only a paramagnetic behavior was observed in this range [see Fig. 6(b)].[9] This disappearance of ferromagnetism cannot be explained by assuming a 1% solubility limit for Co in SnO_2 because (i) the ferromagnetic component due to the soluble part of the doped Co should not be destroyed or overwhelmed by the weak paramagnetic component of the segregated Co_3O_4 formed for $x>0.01$, (ii) the orthorhombic SnO_2 fraction in the samples, lattice parameters, band gap energy, particle size, and shape of the $Sn_{1-x}Co_xO_2$ particles (shown in Figs. 1 and 2) continued to change with x for $x>0.01$ indicating >1% Co solubility in SnO_2, (iii) the observed disappearance of the Raman peaks [Fig. 3(c)] for $x>0.01$ is unlikely to happen if additional Co doping is not taking place, and (iv) no evidence of any change in the oxidation state of Co or Sn is observed in the XPS measurements for $x\geqslant 0.01$.

The appearance of ferromagnetism in $Sn_{1-x}Co_xO_2$ samples with $x\leqslant 0.01$ and its complete absence at higher Co concentrations can be qualitatively understood by comparing the changes in the magnetic and structural properties noticed in the XRD, Raman, and TEM studies of the 600 °C prepared samples. As shown in the previous sections, for $x\leqslant 0.01$ the SnO_2 lattice contracts resulting in the reduction of the distance between nearby Co^{2+} spins and possibly triggering a ferromagnetic coupling. Substitution of Sn^{4+} ions (octahedrally coordinated with six nearest oxygen neighbors) in SnO_2 with Co^{2+} ions will result in the creation of oxygen vacancies and additional charge carriers. It is not clear if this ferromagnetic ordering is carrier mediated[1,2] or via other mechanisms such as the one based on localized defects (F centers) proposed recently by Coey *et al.*[11] Increasing the Co doping to $\geqslant$3% results in a rapid expansion of the SnO_2 lattice and significant structural disorder indicated by the rapid broadening and disappearance of the Raman peaks [Fig. 3(b)]. Such enormous structural changes might have destroyed the ferromagnetic ordering since the magnetic exchange interaction is extremely sensitive to the distance between the interacting spins.

It may be noted that the ferromagnetic regime of $Sn_{1-x}Co_xO_2$ with $x\leqslant 0.01$ corresponds to the compositions for which the SnO_2 lattice contracts [see Figs. 6(b) and 6(c)]. This might suggest that the observed ferromagnetism may be related to internal pressure changes. Changes in the internal or external lattice volume/pressure have been reported to produce ferromagnetism in itinerant electron metamagnets.[27–29] For example, Yoshimura and Nakamura[27] reported a transition from Pauli paramagnetism to ferromagnetism in $Y(Co_{1-x}Al_x)_2$ at a critical doping concentration of $x\sim 0.12$ due to changes in the internal pressure. Similarly, a ferromagnetic to paramagnetic transition was observed in this system by applying external pressure exceeding a critical pressure.[27] Thus more investigations are required to understand the exact role of structural changes and internal pressure differences and the role of oxygen stoichiometry vis à

vis the preparation conditions in controlling the observed ferromagnetism of $Sn_{1-x}Co_xO_2$. It is hoped that this work will stimulate such investigations.

IV. SUMMARY AND CONCLUSIONS

Combined XRD, Raman, optical, XPS, and magnetic studies show that the RTFM in Co-doped tin oxide powders results from the $Sn_{1-x}Co_xO_2$ phase. Substitution of Sn^{4+} ions with Co^{2+} ions results in contraction of the SnO_2 lattice and reduction in the oxygen content, triggering ferromagnetic interactions. For $x \geqslant 0.03$, a rapid expansion of the SnO_2 lattice, presumably due to interstitial incorporation of Co^{2+}, destroys the ferromagnetism. This also results in the conversion of the spherical equiaxed SnO_2 particles to elongated nanorods with aspect ratio ~ 3.

ACKNOWLEDGMENTS

This research was supported in part by grants from the Research Corporation (CC5832), Petroleum Research Fund (PRF Grant No. 41870-AC10), NSF-Idaho-EPSCoR program (EPS Grant No. 0132626), and the DOE-EPSCoR program (Grant No. DE-FG02-04ER46142). A portion of the research described in this paper was performed in the Environmental Molecular Sciences Laboratory, a national scientific user facility sponsored by the Department of Energy's Office of Biological and Environmental Research and located at Pacific Northwest National Laboratory.

*Author to whom all correspondence should be addressed; Email address: apunnoos@boisestate.edu

[1] T. Dietl, H. Ohno, F. Matsukura, J. Cibert, and D. Ferrand, Science **287**, 1019 (2000); T. Dietl, H. Ohno, F. Matsukura, Phys. Rev. B **63**, 195205 (2001).

[2] H. Katayama-Yoshida and K. Sato, J. Phys. Chem. Solids **64**, 1447 (2003); Semicond. Sci. Technol. **17**, 367 (2002).

[3] Y. Matsumoto *et al.*, Science **291**, 854 (2001).

[4] W. K. Park, R. J. Ortega-Hertogs, J. S. Moodera, A. Punnoose, and M. S. Seehra, J. Appl. Phys. **91**, 8093 (2002).

[5] S. A. Chambers and R. F. C. Farrow, Mater. Res. Bull. **28**, 729 (2003), and references therein; S. J. Pearton *et al.*, J. Appl. Phys. **93**, 1 (2003) and references therein.

[6] J. D. Bryan, S. M. Heald, S. A. Chambers, and D. R. Gamelin, J. Am. Chem. Soc. **126**, 11640 (2004).

[7] P. Sharma *et al.*, Nat. Mater. **2**, 673 (2003).

[8] P. V. Radovanovic and D. R. Gamelin, Phys. Rev. Lett. **91**, 157202 (2003).

[9] A. Punnoose, J. Hays, V. Shutthanandan, and V. Gopal, Appl. Phys. Lett. **85**, 1559 (2004).

[10] S. B. Ogale, R. J. Choudhary, J. P. Buban, S. E. Lofland, S. R. Shinde, S. N. Kale, V. N. Kulkarni, J. Higgins, C. Lanci, J. R. Simpson, N. D. Browning, S. Das Sarma, H. D. Drew, R. L. Greene, and T. Venkatesan, Phys. Rev. Lett. **91**, 077205 (2003).

[11] J. M. D. Coey, A. P. Douvalis, C. B. Fitzgerald, and M. Venkatesan, Appl. Phys. Lett. **84**, 1332 (2004).

[12] R. Jenkins and R. L. Snyder, *Introduction to X-ray Powder Diffractometry* (Wiley, New York, 1996).

[13] F. J. Lamelas, J. Appl. Phys. **96**, 6195 (2004).

[14] B. Lu, C. Wang, and Y. Zhang, Appl. Phys. Lett. **70**, 717 (1997).

[15] A. Prodan, N. Vene, F. Sevsek, and M. Hudomalj, Thin Solid Films **147**, 313 (1987).

[16] J. S. Vermaak, C. W. Mays, and D. Kuhlmann-Wilsdorf, Surf. Sci. **12**, 128 (1968).

[17] A. Fouchet, W. Prellier, P. Padhan, Ch. Simon, and B. Mercey, J. Appl. Phys. **95**, 7187 (2004); H. Kimura, T. Fukumura, M. Kawasaki, K. Inaba, T. Hasegawa, and H. Koinuma, Appl. Phys. Lett. **80**, 94 (2002).

[18] G. Kortum, *Reflectance Spectroscopy* (Springer-Verlag, New York, 1969).

[19] Y. R. Park and K. J. Kim, J. Appl. Phys. **94**, 6401 (2003).

[20] Y. D. Kim, S. L. Cooper, M. V. Klein, J.-H. Park, and B. T. Jonker, Phys. Rev. B **50**, 10637 (1994).

[21] D. A. Schwartz, N. S. Norberg, Q. P. Nguyen, J. M. Parker, and D. R. Gamelin, J. Am. Chem. Soc. **125**, 13205 (2003).

[22] A. Dieguez, A. Romano-Rodriguez, A. Vila, and J. R. Morante, J. Appl. Phys. **90**, 1550 (2001).

[23] C. F. Windisch, Jr., G. J. Exarhos, and S. K. Sharma, J. Appl. Phys. **92**, 5572 (2002).

[24] H. C. Choi, Y. M. Jung, I. Noda, and S. B. Kim, J. Phys. Chem. B **107**, 5806 (2003).

[25] S. A. Chambers, R. F. C. Farrow, S. Maat, M. F. Toney, L. Folks, J. G. Catalano, T. P. Trainor, and G. E. Brown, Jr., J. Magn. Magn. Mater. **246**, 124 (2002).

[26] J. F. Moulder, W. F. Stickle, P. E. Sobol, and K. D. Bomben, *Handbook of X-Ray Photoelectron Spectroscopy* (Perkin-Elmer, Eden Prairie, MN, 1992).

[27] K. Yoshimura and Y. Nakamura, Solid State Commun. **56**, 767 (1985).

[28] J. G. M. Armitage, R. G. Graham, P. C. Riedi, and J. S. Abell, J. Phys.: Condens. Matter **2**, 8779 (1990).

[29] N. H. Duc and T. Goto, in *Handbook on the Physics and Chemistry of Rare Earths*, edited by K. A. Gschneidner, Jr. and L. Eyring (Elsevier, Amsterdam, 1999), Vol. 26, pp. 178.